Accuracy Comparison of Frequency and ROCOF Dynamic Estimators under Contingencies

Guglielmo Frigo
Federal Institute of Metrology
Bern-Wabern, Switzerland
guglielmo.frigo@metas.ch

David Macii
University of Trento
Trento, Italy
david.macii@unitn.it

Dario Petri
University of Trento
Trento, Italy
dario.petri@unitn.it

Abstract

The measurement of frequency and Rate of Change of Frequency (ROCOF) is essential for power system monitoring and control. As known, the Phasor Measurement Units (PMUs), especially those based on dynamic estimators, can perform high-rate frequency and ROCOF measurements, thus improving system observability. Indeed, many monitoring and control applications rely on the comparison or aggregation of such measurements, but do not consider their inherent uncertainty. However, the actual accuracy of existing algorithms under contingencies, as well as the accuracy requirements in such conditions are often unclear. In this paper we present a thorough comparison of frequency and ROCOF estimation accuracy of three dynamic PMU algorithms just before and after the occurrence of a contingency. Extensive simulation results in two realistic scenarios confirm that, with a minimum Signal-to-Noise Ratio (SNR) of 60 dB and a four-cycle data record length, the measurement results are rather consistent. Under stable conditions, the frequency and ROCOF errors generally lie within the limits of the IEEE/IEC Standard 60255-118-1:2018, while after contingency, the measurement uncertainty may grow by about one order of magnitude. The presented results pave the way to the use of data fusion techniques to aggregate frequency and ROCOF values over a given area.

Keywords

Phasor Measurement Unit (PMU), Frequency measurement, Rate-of-Change-of-Frequency (ROCOF) measurement, measurement uncertainty, performance evaluation.

I. Introduction

Modern power systems are characterized by an ever-increasing penetration of distributed generation and renewable energy sources (RESs) [1]. These resources are typically interconnected via dedicated power converters that do not contribute to the overall rotational inertia [2], [3]. As a consequence, the power systems are prone to sudden transient conditions that may lead to quality degradation or even interruption of service [4]. In such a challenging scenario, a distributed measurement infrastructure is needed to support power systems monitoring and control [5]. As known, the Phasor Measurement Units (PMUs) are part of the backbone of this infrastructure as they perform synchronized measurements of ac voltage and current phasor, frequency and rate of change of frequency (ROCOF) [6]. Each PMU measurement value is time-stamped on a local or global time scale that must be traceable to the Coordinated Universal Time (UTC). In a Phasor Data Concentrator (PDC), it is possible to aggregate and compare measurement data with the same time-stamps and infer useful information about system operating conditions [7]. The IEC/IEEE Standard 60255-118-1:2018 (briefly called PMU Std in the following) introduces two performance classes (P- and M-class) [8], that are intended for protection and measurement applications, respectively. For each class, the PMU Std specifies both a set of testing conditions and the corresponding performance targets in terms of Total Vector Error (TVE), Frequency Error (FE) and ROCOF Error (RFE). However, the compliance with the PMU Std requirements does not guarantee adequate performance in real-world applications [9], [10].

This is true especially in the case of frequency and ROCOF measurements. Such parameters are of paramount importance to assess the level of stability of a power system. The ac voltage frequency depends on the balance between power generation and consumption, while the voltage ROCOF is related to the system inertial response [11]. By accurately measuring the evolution of frequency and ROCOF over time, unexpected or even dangerous operating conditions can be promptly detected and suitably mitigated [12]. For instance, frequency and ROCOF measurements are typically employed in under-frequency load shedding and load restoration routines [13]. Unfortunately, both frequency and, above all, ROCOF are very sensitive to wideband noise [14]. Moreover, the choice of reasonable ROCOF accuracy limits is still a matter of debate, due to the strong variability of ROCOF measurement uncertainty in testing conditions other than those reported in the PMU Std, especially when fast transients occur [15].

Although the actual frequency and ROCOF values depend on the grid topology as well as on the bus where a PMU is installed, it is usually reasonable to assume that such values are quite comparable over a broad area unless some severe event occurs. For this reason, aggregating (e.g., through a plain arithmetic average) the frequency and ROCOF values collected from multiple distributed PMUs is a quite common practice [16], [17]. However, such practice relies on the hidden assumption that

also the PMU measurement uncertainties are comparable, which is not sure at all, especially if the operating conditions differ from those specified in the PMU Std.

In this paper the frequency and ROCOF estimation accuracy of three state-of-the-art dynamic estimators for PMUs are compared in real-world scenarios. To this aim, both the observation interval length (which is a key parameter, common to all algorithms) and two crucial influence quantities such as wideband noise floor and harmonic distortion level are varied. The proposed study is focused on dynamic estimators only (which will be briefly recalled in Section II), since they are more suitable to track possible time-varying changes of synchrophasor, frequency and ROCOF over time [18]. For the sake of simplicity and brevity, the reported analysis relies on two case studies consisting just of a few buses each, but it could be extended to larger power grids regardless of the type contingency occurred. The accuracy of the three dynamic estimators, as well as the distributions of frequency and ROCOF errors, are then analyzed to provide a valuable performance comparison under both stationary and non-stationary conditions. The corresponding Monte Carlo simulation results are reported in Section III. The purpose of this analysis is to assess to what extent the frequency and ROCOF measurements performed by different PMUs are consistent when a severe contingency affects the actual frequency and ROCOF values either in a similar way (case study A) or in a rather different way (case study B), thus paving the way to possible criteria to support more sensible decisions on when area-level data fusion should be performed. In this respect, some crucial preliminary remarks are outlined in Section IV.

II. Overview of Dynamic PMU Estimators

The IEEE/IEC Standard 60255-118-1:2018 relies on the assumption that the transmission systems are characterized by high inertia and slow variations. In systems with lower inertia, the PMUs are expected to face much faster dynamics and higher distortion levels [19]. For this reason, several recent research activities were focused on the development of dynamic synchrophasor estimation algorithms able to trade accuracy for responsiveness [18], [20]. Most algorithms rely on the assumption that the synchrophasor of the fundamental component is a time-varying complex-valued function that, around a given reference time-stamp $t_r = \frac{n_r}{f_s}$ (where f_s is the PMU sampling rate, chosen as a multiple of the nominal signal frequency f_0), can be approximated by its Taylor's series truncated to a given order (usually the second), i.e.

$$P(t_r+\Delta t)=X(t_r+\Delta t)e^{j\theta(t_r+\Delta t)} \approx p_{0,r}+p_{1,r}n+p_{2,r}n^2 \tag{1}$$

where $X(\cdot)$ is the Root Mean Square (RMS) value of the fundamental component at a given time, $\theta(\cdot)$ is the synchrophasor instantaneous phase angle at the same time, and $\Delta t = \frac{n}{f_s}$ (with $-\frac{N-1}{2} \leq n \leq \frac{N-1}{2}$) is the time offset (expressed in sampling intervals) from the reference time-stamp within a data record consisting of $N = C\frac{f_s}{f_0} + 1$ samples (where f_0 is the nominal ac frequency and C is an integer number of fundamental cycles). Finally, coefficients $p_{k,r} = \frac{1}{k!f_s}\frac{d^k P}{dt}\Big|_{t_r}$ are proportional to $k-$th order derivative of the dynamic synchrophasor (1) computed at t_r. Note that $p_{0,r} = P(t_r)$ is the synchrophasor value at the reference time t_r. By using this general model of the fundamental synchrophasor (which is still valid even in the presence of harmonic distortion), it is shown in [21] that the frequency and ROCOF at time t_r can be estimated from

$$\hat{f}(t_r) = \hat{f}_0 + \frac{f_s}{2\pi|\hat{p}_{0,r}|^2}\mathrm{Im}(\hat{p}_{1,r}\hat{p}^*_{0,r}) \tag{2}$$

$$\hat{R}(t_r)=\frac{f_s^2}{\pi|\hat{p}_{0,r}|^2}\left[\mathrm{Im}(\hat{p}_{2,r}\hat{p}^*_{0,r})-\frac{\mathrm{Re}(\hat{p}_{1,r}\hat{p}^*_{0,r})\mathrm{Im}(\hat{p}_{1,r}\hat{p}^*_{0,r})}{|\hat{p}_{0,r}|^2}\right] \tag{3}$$

where $\hat{\cdot}$ refers to estimated quantities, * denotes the conjugate value of a complex number, and functions $\mathrm{Re}(\cdot)$, $\mathrm{Im}(\cdot)$ return the real and imaginary parts, respectively, of a complex quantity. In the rest of this paper, three different state-of-the-art algorithms are considered to estimate $\hat{p}_{0,r}$, $\hat{p}_{1,r}$ and $\hat{p}_{2,r}$.

A. Tuned Lightweight Taylor-Fourier Transform

The Tuned Lightweight Taylor-Fourier Transform (TLTFT) estimator presented in [22] aims at reducing the computational complexity of the Taylor-Fourier Transform (TFT) that was primarily conceived for dynamic multi-harmonic estimation [23]. The basic idea is to estimate not only the synchrophasor, the frequency and the ROCOF of the fundamental component, but also the synchrophasors of a variable number of low-order harmonics, when they are expected to perturb the estimates of the fundamental parameters significantly. For this reason, other expressions similar to (1), but related to low-order harmonics and with the respective Taylor's series truncated to order 0 (to keep the computational complexity low) are used to build the vector of parameters to be estimated.

The TLTFT consists of two steps that can partly run in parallel to reduce the input-output processing latency. In the first stage, the input data record consisting of about C fundamental cycles is filtered by a plain six-order elliptic filter to attenuate possible disturbances. The filter output sequence is element-wise multiplied by a Maximum Image Rejection (MIR) window [24], and then it is processed by a standard Interpolated Discrete Fourier Transform (IpDFT) to extract the static off-nominal frequency deviation of the fundamental tone [25]. Such a relative frequency offset is then used to tune the coefficients of the following TLTFT system matrix.

In the second stage of the algorithm, the original (i.e., unfiltered) input data record is processed by a linear weighted least-squares estimator. The number of unknowns depends on the number of observed cycles. In particular, the vector of unknowns (initially composed by the real and imaginary parts of coefficients $p_{k,r}$ only, for $k = 0, 1, 2$) is augmented by including the real and imaginary parts of the synchrophasors of the harmonics till a given order. The smaller the number of observed cycles, the greater the number of harmonic components to be estimated becomes. In this way, the influence of low-order harmonics on the estimates of the fundamental parameters can be mitigated [22].

The data record samples are weighted by the square-root of the coefficients of a Hann or an MIR window function to smooth the Taylor series' truncation errors at the endpoints of an observation interval. The elements of the linear system matrix used to implement the least-squares estimator are computed by expressing the multi-harmonic signal model as a function of the Taylor series' coefficients. Such elements also depend on the actual frequency values of the fundamental and of all the harmonic components included in the model. Such values are adjusted by using the frequency deviations estimated by the preliminary IpDFT. The weighted least-squares solutions $\hat{p}_{k,r}$ of the linear system are finally plugged into (2) and (3) to estimate fundamental frequency and ROCOF. One of TLTFT main advantages is that the fundamental parameters are computed in one-shot, i.e., with no iterations.

B. Interpolated Dynamic Discrete Fourier Transform

The Interpolated Dynamic Discrete Fourier Transform (IpD2FT) is an iterative algorithm that, in its original formulation [26], estimates the fundamental synchrophasor in the frequency domain, while compensating for the effect of possible off-nominal static frequency deviations. The IpD2FT relies on the windowed discrete Fourier transform of an input data record. In particular, the spectral samples of the windowed data record (computed at both the nominal fundamental frequency bin and at the ± 1 nearby frequency bins) are set equal to the values resulting from the discrete-time Fourier transform of (1). As a result, if the complex conjugate spectral samples are also considered, a linear system of six equations in the six unknowns $p_{k,r}$ and $p^*_{k,r}$ (for $k = 0, 1, 2$) can be built. The coefficients of the linear system matrix depend on the chosen window function (usually the Hann window is adopted) and on the fundamental frequency value, which is initially set to the nominal value (i.e., 50 Hz or 60 Hz). Once the values of $\hat{p}_{k,r}$ and $\hat{p}^*_{k,r}$ for $k = 0, 1, 2$ result from the solution of the system of equations, the fundamental frequency is also estimated through (2). Such a frequency value is used to update the coefficients of the linear system matrix, so that the values of $\hat{p}_{k,r}$ and $\hat{p}^*_{k,r}$ can be recomputed. This iterative procedure is repeated till when the estimated fundamental frequency value no longer changes significantly. Usually, the algorithm converges within a few iterations.

C. Compressive Sensing Taylor-Fourier Multifrequency

Likewise the TLTFT, also the Compressive Sensing Taylor-Fourier Multifrequency (CS-TFM) estimator relies on the TFT model that was suitably modified and generalized in order to deal with multi-tone signals with arbitrary frequency (i.e., not only harmonics) [27]. The algorithm performance strongly depends on the components included in the TFM model. In its original formulation, a CS routine identifies the signal support as the set of frequencies associated to the most significant spectral components with a resolution better than 0.5 Hz. However, such an implementation is particularly demanding in terms of computational resources. The improved solution described in [28] provides a good trade-off between accuracy and complexity. In particular, an orthogonal matching pursuit algorithm identifies the fundamental frequency with a resolution of 0.4 Hz. If $C \geq 4$ cycles, the TFM model is augmented by including the first four most significant sinusoidal tones. This solution is compliant with both P- and M-class requirements when the observation interval length is set to five nominal cycles [28].

III. Simulation results

In the proposed analysis, we consider two case studies as representatives of plausible frequency and ROCOF variations due to power system contingencies. A PMU is supposed to be installed at every bus (five buses in the former case study and three buses in the latter one). For the sake of simplicity and with no loss of generality, the Signal-to-Noise Ratio (SNR) of the acquisition stage and the sampling rate of all PMUs (i.e., $f_s = 5$ kHz) are assumed to be the same. In each simulation run, a single PMU algorithm at a time (among those described in Section II) is adopted. In this way, the contribution of each estimation algorithm to frequency and ROCOF measurement uncertainty can be analyzed separately. In all cases, the measurement noise is modelled as an additive white Gaussian noise, with zero mean and different variance values to keep the Signal-to-Noise Ratio (SNR) under control. For each case study, two possible scenarios are considered. In the first one, the fundamental component is affected by wideband noise only. In the second one, third-, fifth- and seventh-order harmonics are added with a magnitude of 2.5, 1.25 and 0.75%, respectively, so that the Total Harmonic Distortion (THD) is approximately 3%.

A. Case Study A: Modified IEEE 5-bus test system

The Case Study A refers to a modified version of the IEEE 5-bus test system. In particular, a sudden Under-Frequency Load Shedding (UFLS) operation is performed, as further discussed in [29]. In this way, the frequency and ROCOF estimation accuracy of different kinds of PMUs can be evaluated in both stationary and dynamic conditions.

Fig. 1(a)-(b) shows the actual values of frequency and ROCOF, respectively, as a function of time. The simulation (performed in Matlab Simulink) starts with the power system operating in close-to-nominal conditions: the frequency slightly fluctuates around

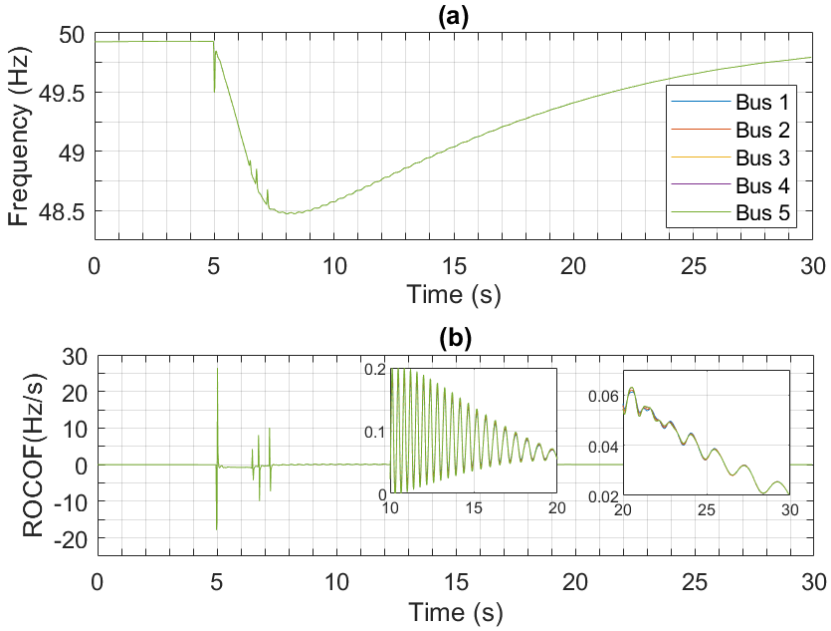

Fig. 1: Actual values of instantaneous frequency (a) and ROCOF (b) in the IEEE 5-bus test case study. In (b), the inset plots show the ROCOF values during two consecutive load restoration actions.

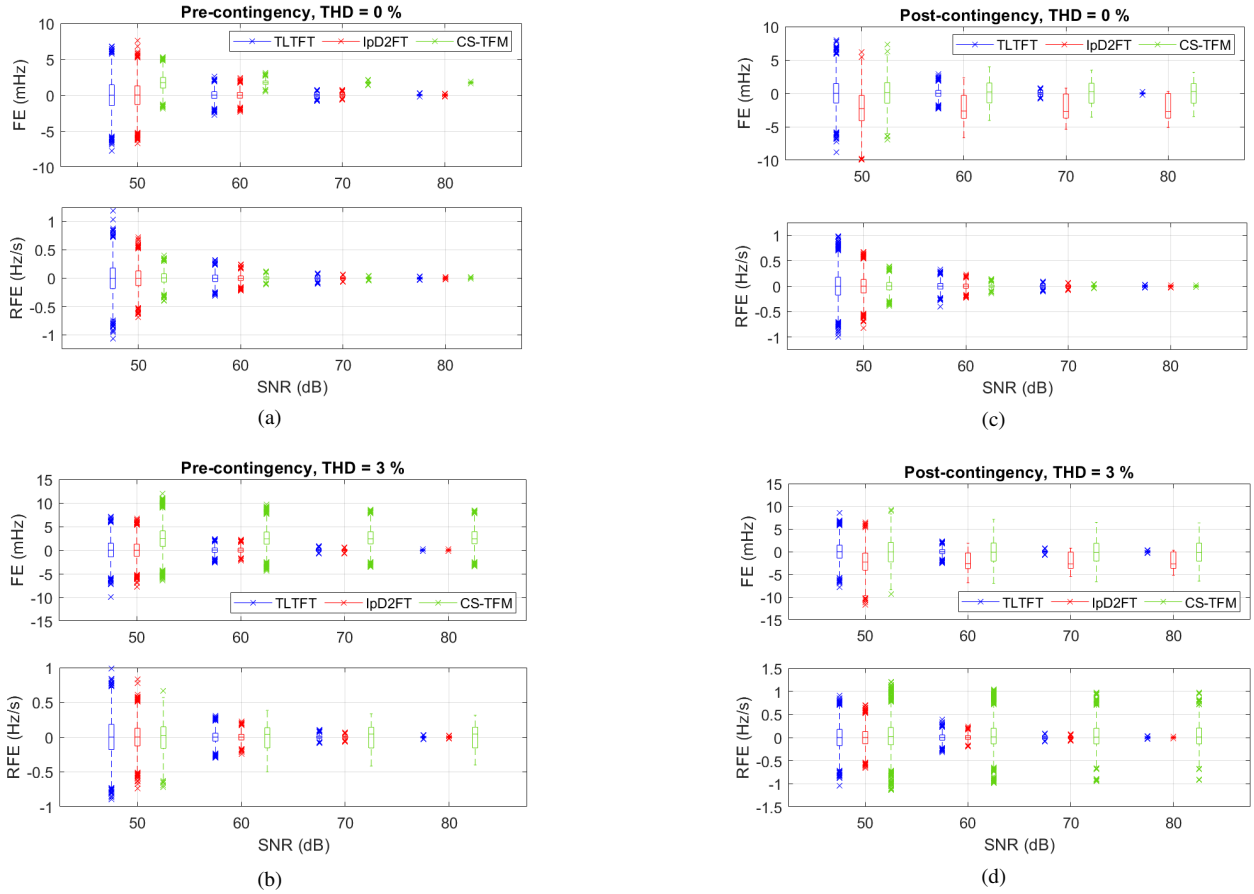

Fig. 2: Box-and-whiskers plots of the FE and RFE values obtained with different dynamic estimators over four-cycle-long data records for increasing SNR values, before (on the left) and after (on the right) the simulated contingency in the IEEE 5-bus case study. The results in (a)-(c) are obtained assuming that no harmonic distortion is present, where in (b)-(d) the THD is 3%.

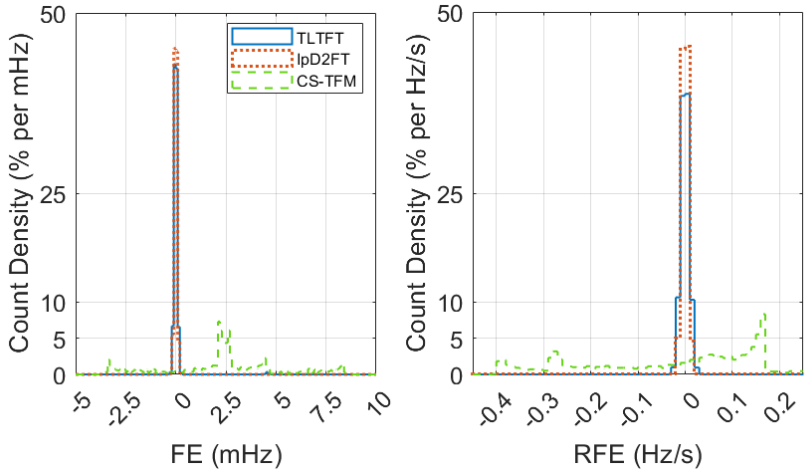

(a)

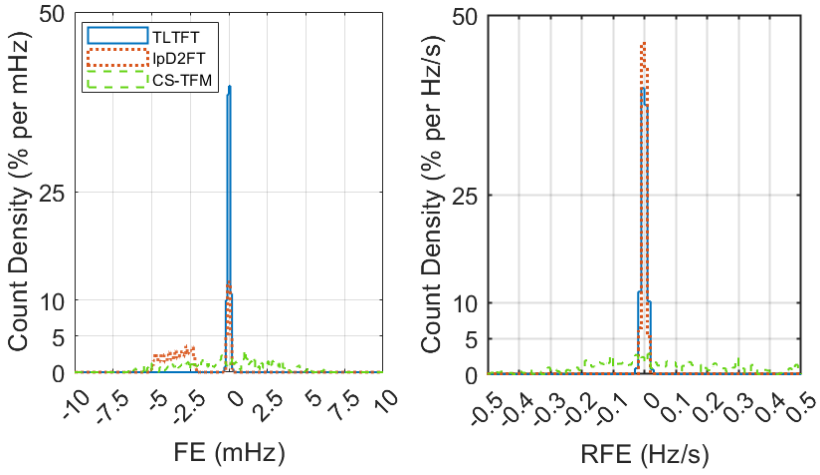

(b)

Fig. 3: Density plots of the FEs and RFEs of the three PMU algorithms before (a) and after (b) the contingency in Case Study A using four-cycle-long windows and assuming SNR = 80 dB and THD = 3%.

the nominal value (i.e., 50 Hz), while the ROCOF is negligible. At $t = 5$ s, the output power of the generator at bus 2 is partially tripped by 300 MW. Excluding the discontinuities due to the load shedding, the contingency causes a rapid frequency drop at an average ROCOF of nearly -0.7 Hz/s. The prompt intervention of the UFLS control action arrests the frequency drop within 3 s, and initiates the load restoration procedure. At each load shed, the frequency is perturbed and a significant sudden ROCOF change can be noticed. On the other hand, the load restoration is characterized by a dampened oscillatory trend, as shown by the two inlet plots. In a first stage, the ROCOF oscillates within 0 and 0.2 Hz/s with a period of 0.2 s. In a second stage, the oscillation is less visible and the ROCOF exhibits a linear trend with a slope of about -0.01 Hz/s^2. Since, the frequency and ROCOF values at all five buses are very similar, this case study is a good example to evaluate to what extent the PMUs return consistent results when data are collected in different nodes.

Fig. 2 shows the box-and-whiskers plots of both the Frequency Errors (FE) and the ROCOF Errors (RFE) obtained with the three PMU estimators described in Section II over $C = 4$ cycles for increasing SNR values. The plots refer to the errors collected at bus 1 over 100 repeated runs before the contingency [Fig. 2(a)-(b)] and immediately after completing the load restoration procedure [Fig. 2(c)-(d)], that in Fig. 1(b) correspond to the time intervals $[0, 5)$ s and $[10, 15)$ s, respectively. In Fig. 2(a)-(c) just the effect of wideband noise is considered, while in Fig. 2(b)-(d) the results obtained with THD = 3% are reported. The FE and RFE distributions at the other buses are very similar, since in this example the impact of the simulated UFLS contingency on the actual frequency and ROCOF values at all buses is almost the same, as confirmed by the simulation results shown in Fig. 1(a)-(b). Therefore, the FE and RFE errors at buses other than bus 1 are not shown here for the sake of brevity.

Although the testing conditions are totally different from those specified in the PMU Std, if SNR ≥ 60 dB and the harmonic distortion is negligible, both the FE and RFE values are generally within the limits of the PMU Std (i.e., 5 mHz and below 0.4 Hz/s), except for a few outliers. The impact of the additional harmonic distortion is negligible in most cases. In fact, only the CS-TFM technique seems to be slightly more sensitive to harmonics. This is probably due to the finite resolution of the fundamental frequency initial guess, that results in an imperfect mitigation of the harmonic injections.

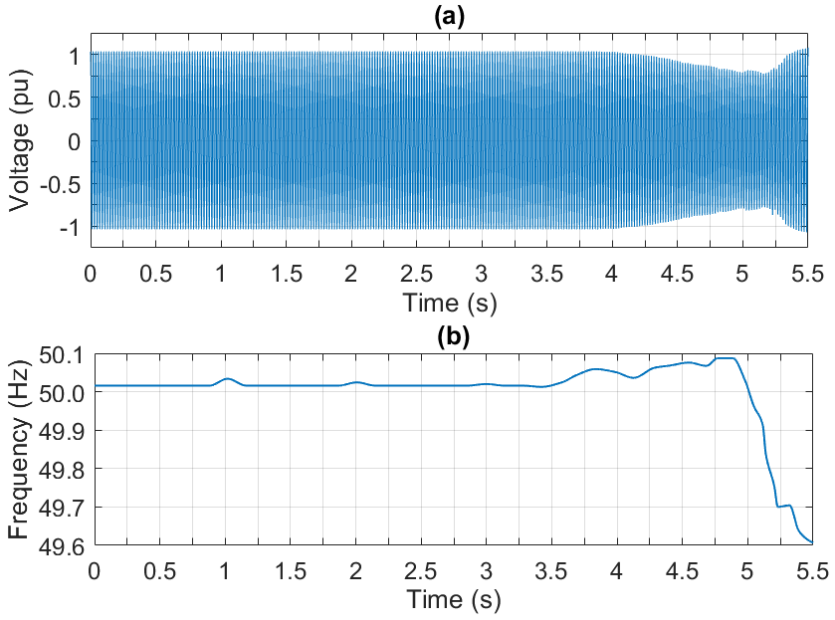

Fig. 4: Voltage waveform (a) and actual frequency values (b) measured on one phase of the Temelli substation (Turkey) just before and after the power outage of March 31, 2015.

After the contingency, despite the load restoration actions, all algorithms converge quite quickly to accuracy levels comparable with those observed just before the contingency. Of course, the number of outliers is a bit higher, especially in the RFE values, maybe due to the sudden changes occurring when the load restoration actions are performed. The CS-TFM algorithm is slightly more affected than the other estimators by the considered contingency. However, the FE values returned by the IpD2FT estimator are those that are most noticeably in non-stationary operating conditions.

While the RFE distributions are almost normal and with zero mean in most cases, the FE distributions exhibit a rather heterogeneous behavior. In particular, the frequency estimates of the CS-TFM algorithm before the contingency and those returned by the IpD2FT algorithm after the contingency are biased and the respective FE distributions may exhibit a multi-modal shape. Similar considerations hold for Fig. 3(a)-(b), that show the density plots of FE and RFE values before and after the contingency of Case Study A. With reference to Fig. 1, the upper lower plots plots refer to the time intervals $[0, 5)$ s and $[10, 15)$, respectively. For this analysis, the window length, the SNR and the THD are set to $C = 4$ cycles, 80 dB, and 3%, respectively. For the sake of comparability, the horizontal axis resolution is fixed: 0.1 mHz for FEs, and 0.01 Hz/s for RFEs. Before the contingency, distributions of the TLTFT and IpD2FT FE and RFE values exhibit nearly coincident distributions, while after the contingency their results start to diverge, particularly in the FE case. Conversely, the CS-TFM distributions are not always centered around zero and the distribution is generally spread over a broader interval.

B. Case Study B: 2015 Turkey power outage

The second case study analyzed in the paper refers to a major power outage occurred in Turkey on March 31, 2015 [30]. Due to the trip of an overloaded line, the Turkish transmission system was split into two subsystems. In the western one, a sudden -21% power deficit caused the loss of synchronism with the Central Europe system.

Fig. 4 shows the voltage signal of one phase and the corresponding actual instantaneous frequency in (a) and (b), respectively, before and after the occurred contingency. The frequency and ROCOF values were reconstructed from the data collected at the Temelli substation in Turkey, by using the waveform reconstruction procedure described in [31]. In the pre-contingency stage, the system is rather stable. At $t = 4$ s, a rapid fall of the voltage level occurs and the frequency tends to exhibit an irregular pattern. At $t = 5$ s, the three interconnection lines with the Bulgarian and Greek systems are also tripped. As a result, the frequency rapidly drops to 49.6 Hz, with an average ROCOF of -3 Hz/s.

Fig. 5(a)-(b) shows the 99th percentiles of FE and RFE values obtained assuming to install a PMU running the TLTFT, the IpD2FT or the CS-TFM algorithm at the Temelli substation. In this case, the study is performed by using data records of increasing size (i.e., for $C = 2$, 4 and 6 cycles, respectively). As expected, as C grows the estimation accuracy of a given algorithm improves, However, also latency and computational burden grow worse. For $C = 4$ or 6 cycles errors are reasonable both before and after the contingency. However, in this case the post-contingency FE and RFE values grow by about one order of magnitude compared with the pre-contingency ones due to the large inherent variability of the measured quantities. At a glance, the TLTFT algorithm is the worst one in stationary conditions and the best one in transient condition, whereas the CS-TFM exhibits the opposite trend. However, the results at other buses (not reported for space constraints) do not confirm this behavior. Sometimes, the IpD2FT and the CS-TFM estimates are affected by occasional biases that should be estimated and corrected.

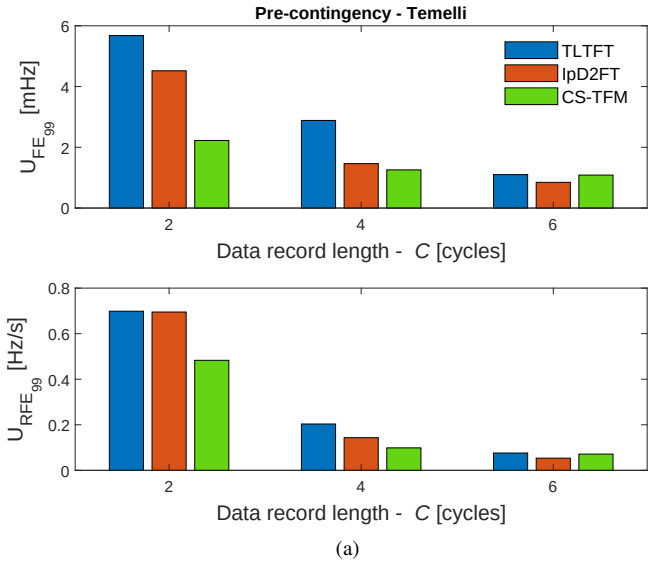

(a)

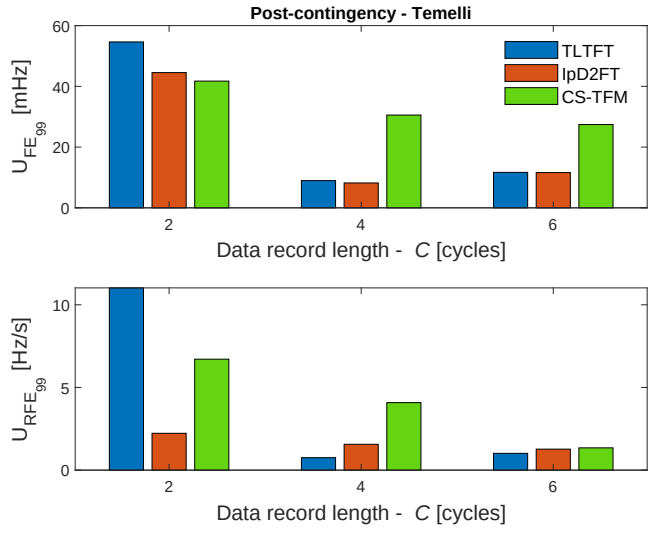

(b)

Fig. 5: 99th percentiles of frequency and ROCOF errors of the three PMU algorithms under test before (a) and after (b) the contingency of Case Study B. The data records' size is varied between 2 and 6 nominal cycles.

IV. Conclusions

This paper presents a performance comparison of three dynamic estimators for PMUs when they are used to measure frequency and ROCOF in real-world operating conditions, especially during contingencies. If at least four-cycle-long data record are observed and if the overall signal-to-noise ratio is not lower than 60 dB, the measurement results obtained with different algorithms are rather consistent, i.e., characterized by a comparable uncertainty range that mainly depends on the intrinsic variability of the measurand either before or after the occurrence of the contingency. Therefore, unless the actual frequency and ROCOF values at different buses drift away from one another due to the consequences of the fault, the fusion of multiple PMU data is expected to greatly improve the accuracy of frequency and ROCOF estimation under contingencies, thus mitigating the risk of making wrong decisions and supporting prompter control actions. Some research activities on how to perform frequency and ROCOF data fusion are currently ongoing, possibly compensating for possible frequency estimation biases, if present. In this regard, a Kalman filter could be used: if the frequency and the ROCOF at different buses are regarded as the state variables of the system, the corresponding consistent PMU measurement data could be used in the update step.

Acknowledgements

This work is supported by the SFOE QUINPORTION Research Program under Grant SI/502415 and by the European Union under NextGenerationEU, PRIN 2022 (Prot. no. 20224X2AYH, CUP E53D23000420006).

REFERENCES

[1] M. Paolone *et al.*, "Fundamentals of power systems modelling in the presence of converter-interfaced generation," *El. Power Sys. Res.*, vol. 189, pp. 1–35, 2020.

[2] H. Saad *et al.*, "Modular multilevel converter models for electromagnetic transients," *IEEE Trans. on Power Delivery*, vol. 29, no. 3, pp. 1481–1489, 2014.

[3] S. O. Muhanji *et al.*, "Distributed control for distributed energy resources: Long-term challenges and lessons learned," *IEEE Acc.*, vol. 6, pp. 32 737–32 753, 2018.

[4] R. Langella *et al.*, "Experimental-based evaluation of pv inverter harmonic and interharmonic distortion due to different operating conditions," *IEEE Trans. Instrum. Meas.*, vol. 65, no. 10, pp. 2221–2233, 2016.

[5] Y. Liu *et al.*, "A distribution level wide area monitoring system for the electric power grid–fnet/grideye," *IEEE Acc.*, vol. 5, pp. 2329–2338, 2017.

[6] J. De La Ree *et al.*, "Synchronized phasor measurement applications in power systems," *IEEE Trans. Smart Grid*, vol. 1, no. 1, pp. 20–27, 2010.

[7] I. Kamwa *et al.*, "Adaptive phasor and frequency-tracking schemes for wide-area protection and control," *IEEE Trans. on Pow. Del.*, vol. 26, no. 2, pp. 744–753, 2011.

[8] *IEEE/IEC International Standard - Measuring relays and protection equipment - Part 118-1: Synchrophasor for power systems - Measurements*, IEEE/IEC IEEE/IEC 60255-118-1, Dec 2018.

[9] G. Frigo *et al.*, "PMU-based rocof measurements: Uncertainty limits and metrological significance in power system applications," *IEEE Trans. Instrum. Meas.*, vol. 68, no. 10, pp. 3810–3822, 2019.

[10] P. S. Wright *et al.*, "Field measurement of frequency and rocof in the presence of phase steps," *IEEE Trans. Instrum. Meas.*, vol. 68, no. 6, pp. 1688–1695, 2019.

[11] G. Chown *et al.*, "System inertia and rate of change of frequency (RoCoF) with ncreasing non-synchronous renewable energy penetration," in *CIGRE - Innovation in the Power Systems industry*, 2018, pp. 32–43.

[12] P. Gupta *et al.*, "Active rocof relay for islanding detection," *IEEE Trans. on Pow. Del.*, vol. 32, no. 1, pp. 420–429, 2017.

[13] Y. Zuo *et al.*, "Impact of synchrophasor estimation algorithms in rocof-based under-frequency load-shedding," *IEEE Trans. Power Syst.*, vol. 35, no. 2, pp. 1305–1316, 2020.

[14] D. Macii *et al.*, "Impact of acquisition wideband noise on synchrophasor measurements: A design perspective," *IEEE Trans. on Instrumentation and Measurement*, vol. 65, no. 10, pp. 2244–2253, 2016.

[15] A. J. Roscoe, "Exploring the relative performance of frequency-tracking and fixed-filter phasor measurement unit algorithms under c37.118 test procedures, the effects of interharmonics, and initial attempts at merging p-class response with m-class filtering," *IEEE Trans. on Instrumentation and Measurement*, vol. 62, no. 8, pp. 2140–2153, 2013.

[16] A. Fuchs *et al.*, "Aggregated models of active distribution networks for stability studies of large transmission systems," *Electric Power Systems Research*, vol. 212, p. 108607, 2022.

[17] NERC, "Fast frequency response concepts and bulk power system reliability needs," [Online] available at: https://www.nerc.com/comm/PC/, March 2020.

[18] G. Barchi *et al.*, "Synchrophasor estimators accuracy: A comparative analysis," *IEEE Trans. on Instrumentation and Measurement*, vol. 62, no. 5, pp. 963–973, 2013.

[19] M. Chakir *et al.*, "Extended c37.118.1 pmu algorithms for joint tracking of fundamental and harmonic phasors in stressed power systems and microgrids," *IEEE Trans. on Power Delivery*, vol. 29, no. 3, pp. 1465–1480, 2014.

[20] CIGRE, "Application of phasor measurement units for monitoring power system dynamic performance," [Online] available at: https://www.e-cigre.org/publications/, September 2017.

[21] J. A. de la O Serna, "Dynamic phasor estimates for power system oscillations," *IEEE Trans. on Instrumentation and Measurement*, vol. 56, no. 5, pp. 1648–1657, 2007.

[22] P. Tosato *et al.*, "A tuned lightweight estimation algorithm for low-cost phasor measurement units," *IEEE Trans. Instrum. Meas.*, vol. 67, no. 5, pp. 1047–1057, 2018.

[23] M. A. Platas-Garza and J. A. de la O Serna, "Dynamic harmonic analysis through taylor–fourier transform," *IEEE Trans. on Instrumentation and Measurement*, vol. 60, no. 3, pp. 804–813, 2011.

[24] D. Macii *et al.*, "Accuracy analysis and enhancement of dft-based synchrophasor estimators in off-nominal conditions," *IEEE Trans. Instrum. Meas.*, vol. 61, no. 10, pp. 2653–2664, 2012.

[25] D. Belega *et al.*, "Fast synchrophasor estimation by means of frequency-domain and time-domain algorithms," *IEEE Trans. Instrum. Meas.*, vol. 63, no. 2, pp. 388–401, 2014.

[26] D. Petri *et al.*, "A frequency-domain algorithm for dynamic synchrophasor and frequency estimation," *IEEE Trans. Instrum. Meas.*, vol. 63, no. 10, pp. 2330–2340, 2014.

[27] M. Bertocco *et al.*, "Compressive sensing of a taylor-fourier multifrequency model for synchrophasor estimation," *IEEE Trans. Instrum. Meas.*, vol. 64, no. 12, pp. 3274–3283, 2015.

[28] G. Frigo *et al.*, "Taylor-Fourier PMU on a real-time simulator: Design, implementation and characterization," in *2019 IEEE Milan PowerTech*, 2019, pp. 1–6.

[29] Q. Walger *et al.*, "Opf-based under frequency load shedding predicting the dynamic frequency trajectory," *Electric Power Systems Research*, vol. 189, p. 106748, 2020.

[30] ENTSO-E, "Report on blackout in Turkey on 31st March 2015," [Online] available at: https://eepublicdownloads.entsoe.eu/, Sept. 2015.

[31] G. Frigo *et al.*, "Tracking power system events with accuracy-based PMU adaptive reporting rate," *International Journal of Electrical Power & Energy Systems*, vol. 153, p. 109384, 2023.